Research Article Vol. 4, No. 1 / 15 January 2021 / OSA Continuum 55

Inverse photonic-crystal-fiber design through geometrical and material scalings

ENRIQUE SILVESTRE,[1,*] AKTHAM TASHTUSH,[1,2] DAVID CASTELLÓ-LURBE,[3] AND MIGUEL V. ANDRÉS[2]

[1] Departament of Optics–ICMUV, Universitat de València, E-46100 Burjassot, Spain
[2] Departament of Applied Physics–ICMUV, Universitat de València, E-46100 Burjassot, Spain
[3] Brussels Photonics, Department of Applied Physics and Photonics, Vrije Universiteit Brussel, Pleinlaan 2, 1050 Brussel, Belgium
[*] enrique.silvestre@uv.es

Abstract: Geometrical and material — i.e., external and internal — scaling symmetries are exploited to obtain approximated analytical expressions for the mode effective index, group index, and chromatic dispersion of a scaled fiber. Our results include material refractive index scaling that changes the numerical aperture. First, the analytical expressions are successfully tested with a conventional step index fiber in a broadband range of wavelengths, from 1 to 2 μm. Then, we establish a procedure to adapt the analytical expressions to photonic crystal fibers (PCFs) and illustrate its application in a triangular PCF with circular holes. These adapted analytical expressions show good agreement with a rigorous numerical solution of the fundamental fiber mode. Finally, we demonstrate how powerful these expressions are for the design of PCFs. In particular, we illustrate our approach designing, in four iterations or less, PCFs with flattened dispersion profile over 300 nm or high dispersion slope over 40 nm, with different chromatic dispersion values.

1. Introduction

The design of waveguides and optical fibers is crucial for achieving high performance in applications such as dispersion compensation [1], parametric amplification [2], wavelength conversion [3,4], and supercontinuum generation in both anomalous [5,6] and normal dispersion regimes [7,8]. One of the most important properties controlling the physical behavior of these optical systems, in both the linear and nonlinear regimes, is chromatic dispersion. The waveguide dispersion not only depends on its constituent materials, but also displays a high sensitivity to changes in geometry (see, e.g., [9]).

Different approaches have been followed to control dispersion properties. They range from the use of empirical relations involving the V-parameter, obtained for PCFs that consist of triangular grids of air holes on a pure silica matrix [10,11] to guided test-and-trial procedures based on, e.g., genetic algorithms [12] or topology optimization [13,14], which can become time-consuming if the parameter space to be explored is not restricted judiciously [15]. In general, the design process requires the minimization of a merit function. When the first derivatives of the merit function are available, gradient-based algorithms are certainly the first choice in multidimensional minimization, as they can dramatically reduce the number of evaluations of the merit function [16,17]. Some of those methods rely on iterative strategies that produce a series of local approximations of the merit function. It is worth noting here that the above methods are compatible with the use of approximate analytical expressions for the waveguide dispersion [9], as well as with any particular mode solver (for instance, [18,19]). Moreover, such theoretical results offer opportunities to calculate the merit function in larger neighborhoods of given values for the set of parameters and thus, to further reduce the number of iterations. In particular, the geometrical scaling symmetry exhibited by guiding systems under certain conditions [20] opens

#408646 https://doi.org/10.1364/OSAC.408646
Journal © 2021 Received 8 Sep 2020; revised 22 Nov 2020; accepted 23 Nov 2020; published 24 Dec 2020

OSA CONTINUUM

the possibility to adjust their optical properties, and has been essential in the design of PCFs [9,16].

In this paper, we generalize the geometrical — or *external* — scaling transformation presented in Ref. [20] by introducing a material — or *internal* — transformation by which the numerical aperture is modified, taking advantage of invariants of the scalar wave equation in non-dispersive media [21]. Next we derive a series of approximated analytical expressions that describe the propagation constant, the group index and the group velocity dispersion in terms of their counterparts in the unscaled system and the corresponding external and internal scale factors. Thus, the calculation of these properties for a given waveguide suffices to obtain analytically those corresponding to scaled versions of the initial waveguide, including both geometrical and material scalings, as we show in conventional fibers and PCFs. Finally, we prove the power of our new results to design photonic crystal fibers featuring different targeted dispersion curves, such as flattened profiles or featuring a high slope, in four iterations or less. These results show up the efficiency of our approach compared to pure brute-force strategies.

2. External and internal scaling symmetries in guiding systems

We start with the 2D wave equation in the weak-guidance approximation [22],

$$\left[\nabla_{\mathrm{t}}^2 + \left(\frac{\omega}{c}\right)^2 n^2(\mathbf{x}_{\mathrm{t}}, \omega)\right] \Psi(\mathbf{x}_{\mathrm{t}}, \omega) = \beta^2(\omega)\Psi(\mathbf{x}_{\mathrm{t}}, \omega), \tag{1}$$

where the subscript t indicates transverse components, $n(\mathbf{x}_{\mathrm{t}}, \omega)$ represents the spatial distribution of the refractive index of a guiding system, Ψ denotes any of the transverse electric (or magnetic) field components and β is its propagation constant. If the system only involves non-dispersive media and the scaling transformation $n^2(\mathbf{x}_{\mathrm{t}}) \mapsto n^2_{[s]}(\mathbf{x}_{\mathrm{t}}) = n^2(\mathbf{x}_{\mathrm{t}}/s)$ is considered, a straight comparison between Eq. (1) for the scaled system and the same equation for the unscaled system with the variable changes $\mathbf{x}_t \mapsto \mathbf{x}_{\mathrm{t}}/s$ and $\omega \mapsto s\omega$ shows that the modes corresponding to the scaled system, $\Psi_{[s]}$, and their propagation constants, $\beta_{[s]}$, meet the direct relationships $\Psi_{[s]}(\mathbf{x}_{\mathrm{t}}, \omega) = \Psi(\mathbf{x}_{\mathrm{t}}/s, s\omega)$ and $\beta^2_{[s]}(\omega) = \beta^2(s\omega)/s^2$ with those of the unscaled system [9,20].

The solution for a more general transformation given by $n^2(\mathbf{x}_{\mathrm{t}}) \mapsto n^2_{[sr]}(\mathbf{x}_{\mathrm{t}}) = r\, n^2(\mathbf{x}_{\mathrm{t}}/s)$, namely, a simultaneous external and internal scaling transformation, is obtained just considering the variable changes $\mathbf{x}_t \mapsto \mathbf{x}_{\mathrm{t}}/s$ and $\omega \mapsto s\sqrt{r}\omega$:

$$\Psi_{[sr]}(\mathbf{x}_{\mathrm{t}}, \omega) = \Psi(\mathbf{x}_{\mathrm{t}}/s, s\sqrt{r}\omega), \tag{2}$$

$$\beta^2_{[sr]}(\omega) = \beta^2(s\sqrt{r}\omega)/s^2. \tag{3}$$

Given a guiding system, hence a refractive-index spatial distribution, Eq. (3) determines the propagation constant (and thus the chromatic dispersion) of *any* scaled system based solely on the calculation of the propagation constant corresponding to the unscaled system. This result can be of utmost importance for fiber design since it allows straightforwardly determining the required scaling in a given fiber to obtain a target optical property.

In practice, the internal scaling transformation typically keeps unchanged the refractive index of one of the constituent materials, the reference material, n_{ref} (e.g., the refractive index of the cladding of a step-index fiber). This scaling transformation can be managed in the wave equation subtracting the term $(\omega/c)^2 n^2_{\mathrm{ref}}(\omega)\Psi$ from both sides of Eq. (1),

$$\left[\nabla_{\mathrm{t}}^2 + \left(\frac{\omega}{c}\right)^2 \Delta n^2(\mathbf{x}_{\mathrm{t}})\right] \Psi(\mathbf{x}_{\mathrm{t}}, \omega) = \Delta\beta^2(\omega)\Psi(\mathbf{x}_{\mathrm{t}}, \omega), \tag{4}$$

where $\Delta\beta^2(\omega) = \beta^2(\omega) - \beta^2_{\mathrm{ref}}(\omega)$, and $\beta_{\mathrm{ref}}(\omega) = (\omega/c)n_{\mathrm{ref}}(\omega)$ is the propagation constant in the reference material. Note that the scaling symmetry will still be valid within a spectral bandwidth

OSA CONTINUUM

where the constituent media present not so different dispersive behavior and, hence, the numerical aperture be approximately constant, i.e., $\Delta n^2(\mathbf{x}_t) = n^2(\mathbf{x}_t, \omega) - n^2_{\text{ref}}(\omega)$. We will show at the end of this section that such an approximation at least holds in the spectral range between 1 μm and 2 μm for a conventional fiber. To be precise, the scaling transformation $\Delta n^2(\mathbf{x}_t) \mapsto \Delta n^2_{[sr]}(\mathbf{x}_t) = r\Delta n^2(\mathbf{x}_t/s)$ implies, along the lines of the derivation of Eq. (3), $\Delta\beta^2_{[sr]}(\omega) = \Delta\beta^2(s\sqrt{r}\omega)/s^2$, and therefore

$$\beta^2_{[sr]}(\omega) = \frac{1}{s^2}\left[\beta^2(s\sqrt{r}\omega) - \beta^2_{\text{ref}}(s\sqrt{r}\omega)\right] + \beta^2_{\text{ref}}(\omega)\,. \tag{5}$$

For a conventional step index fiber, the silica cladding can be chosen as the reference [Fig. 1(a)]. For those systems with nontrivial claddings, as it is the case of photonic crystal fibers, the reference can be the solid core material [Fig. 2(a)]. In both examples, the approximated constancy of the numerical aperture can be noticed.

For guiding systems described within the weak-guidance approximation, Eq. (5) can be simplified. According to the weak-guidance approximation, we can assume that $\beta(\omega)$ is similar to $\beta_{\text{ref}}(\omega)$ [i.e., $\Delta\beta^2(\omega) \approx 2\beta_{\text{ref}}(\omega)\Delta\beta(\omega)$], and, in the same order of approximation, we can consider that the reference propagation constant is weakly dispersive [$\beta_{\text{ref}}(a\omega) \approx a\beta_{\text{ref}}(\omega)$], in such a way that the following expression is reached,

$$\beta_{[sr]}(\omega) \approx \frac{r^{1/2}}{s}\left[\beta(s\sqrt{r}\omega) - \beta_{\text{ref}}(s\sqrt{r}\omega)\right] + \beta_{\text{ref}}(\omega)\,. \tag{6}$$

Furthermore, this approximate result can also be of use within the framework of iterative design strategies, as we will present in the next section, where the refractive-index spatial distribution is progressively modified. By deriving Eq. (6) with respect to frequency once and twice, we obtain the proper approximations for the group index coefficient, β_1, and the group velocity dispersion coefficient, β_2,

$$\beta_{1[sr]}(\omega) \approx r\left[\beta_1(s\sqrt{r}\omega) - \beta_{1,\text{ref}}(s\sqrt{r}\omega)\right] + \beta_{1,\text{ref}}(\omega), \tag{7}$$

$$\beta_{2[sr]}(\omega) \approx sr^{3/2}\left[\beta_2(s\sqrt{r}\omega) - \beta_{2,\text{ref}}(s\sqrt{r}\omega)\right] + \beta_{2,\text{ref}}(\omega)\,. \tag{8}$$

Once the $\beta(\omega)$, $\beta_1(\omega)$ and $\beta_2(\omega)$ functions are known for a specific guiding system within a given spectral range, Eqs. (6), (7) and (8) will allow us to obtain a very good estimation of the dispersive behavior corresponding to any scaled version of that same system for the scaled spectral range.

For the sake of completeness, we can also show the equivalent quadratic expression for the effective refractive index, n_{eff},

$$n^2_{\text{eff}[sr]}(\omega) \approx r\left[n^2_{\text{eff}}(s\sqrt{r}\omega) - n^2_{\text{ref}}(s\sqrt{r}\omega)\right] + n^2_{\text{ref}}(\omega), \tag{9}$$

and the correspoding linear expressions for n_{eff}, the group index, n_g, and the group velocity dispersion, D:

$$n_{\text{eff}[sr]}(\omega) \approx r\left[n_{\text{eff}}(s\sqrt{r}\omega) - n_{\text{ref}}(s\sqrt{r}\omega)\right] + n_{\text{ref}}(\omega), \tag{10}$$

$$n_{g[sr]}(\omega) \approx r\left[n_g(s\sqrt{r}\omega) - n_{g,\text{ref}}(s\sqrt{r}\omega)\right] + n_{g,\text{ref}}(\omega), \tag{11}$$

$$D_{[sr]}(\omega) \approx \frac{r^{1/2}}{s}\left[D(s\sqrt{r}\omega) - D_{\text{ref}}(s\sqrt{r}\omega)\right] + D_{\text{ref}}(\omega)\,. \tag{12}$$

In Fig. 1, we compare the analytical results provided by our Eqs. (10), (11) and (8) (dotted lines) with the numerical results provided by a mode solver (solid lines) for several scalings of a standard step-index fiber (SMF-28). The correspondence between our theorical expressions and the simulations is excellent for n_{eff}, n_g and β_2 over a wide wavelength range between 1 μm and 2 μm. The agreement observed in Fig. 1 together with the simple form of Eqs. (10), (11) and (8) confer great potential to these scale relations for fiber design, as we will show in Section 4.

OSA CONTINUUM

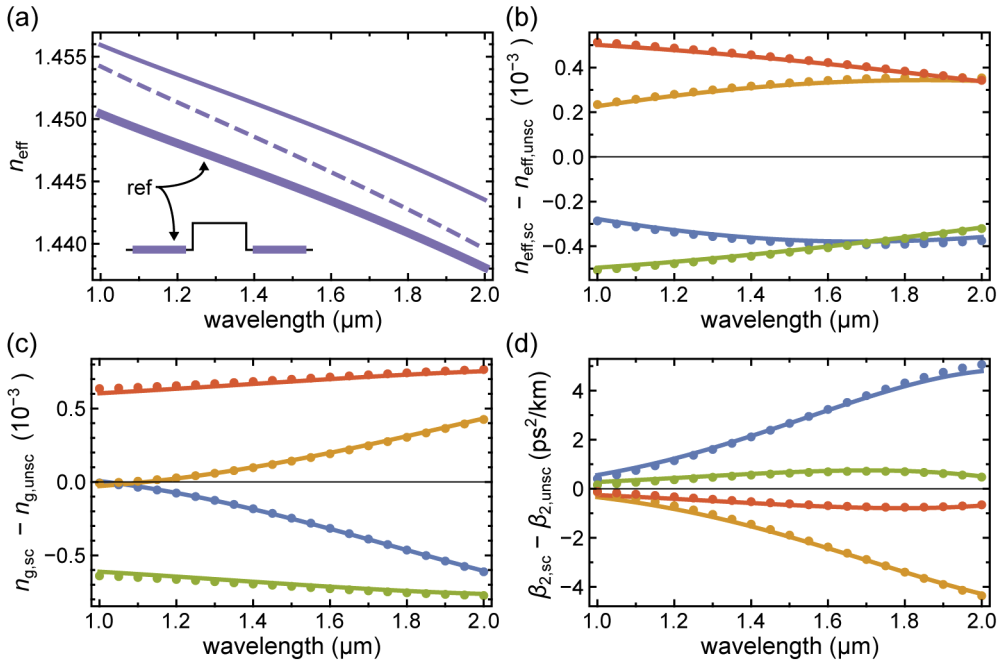

Fig. 1. (a) Effective refractive index of the fundamental mode of a SMF-28 fiber (thin dashed line), refractive index of the core (thin solid line) and the cladding (thick solid line). Variation of n_{eff} (b), n_{g} (c) and β_2 (d) when several scalings (keeping the refractive index of the cladding as the reference for internal scalings) are applied to the fiber: $(s, r) = (0.9, 1)$ [blue], $(1.1, 1)$ [orange], $(1, 0.9)$ [green], and $(1, 1.1)$ [red]; in all cases, both solving completely the mode problem (solid lines) and using the approximated analytical expressions given by Eqs. (10), (11) and (8) (dotted lines). The subscripts `sc` and `unsc` refer to *scaled* and *unscaled*, respectively.

It is worth mentioning that Eq. (12) proves theoretically and generalizes the expression for global scaling in Ref. [16], and ultimately in Ref. [9]. What is more, the successful application of these expressions to the design of photonic crystal fibers [9,16] reveals that our results might be even valid beyond the weak-guidance approximation, in line with the dispersion estimate considered in Ref. [23] for a high-index-contrast integrated waveguide.

OSA CONTINUUM

3. Scaling in photonic crystal fibers

To illustrate our approach in PCFs, here we will focus on triangular PCFs with circular holes, although, unlike other methods [10,11], the procedure can be easily adapted to other geometries with no extra computational effort. A triangular lattice is characterized by the hole radius, a, and the lattice period, or pitch, Λ. A direct application of the external and internal scalings parameterized by s and r to PCFs would lead to new PCFs with pitch $s\,\Lambda$, hole radius $s\,a$, and the material refractive indices — typically, silica, air or both — scaled by a factor r [21]. However, PCFs allow controlling both external *and* internal scalings only by means of their geometry, which is in contrast to conventional fibers. This approach requires a careful application of the formulas derived in the previous section. In particular, an effective step-index-fiber model for PCFs [24,25] can be introduced to define the scaling parameters s and r properly. For such a purpose, we parametrize the PCF by the pitch and the hole-filling fraction of the photonic crystal cladding, $f = (2\pi/\sqrt{3})(a/\Lambda)^2$.

Now, the changes considered in the PCF are a global geometrical scaling, s_g, and a filling fraction scaling, s_f, in such a way that $(\Lambda, f) \mapsto (s_g\Lambda, s_f f)$. The relation between (s_g, s_f) and (s, r) can be determined by the homogenization of the photonic crystal cladding [24]. The core radius of the equivalent step-index fiber can be approximated by $r_0 = \Lambda - a$, with its core index being the same of the PCF matrix, n_{co}, and its cladding index being a simple spatial average of the photonic crystal cladding materials, $n_{\mathrm{cl}}^2 \approx (1-f)n_{\mathrm{co}}^2 + f n_{\mathrm{ho}}^2$ [24,25], where n_{ho} is the refractive index of the material filling the holes. In this way, the square of the numerical aperture, $\mathrm{NA}^2 = n_{\mathrm{co}}^2 - n_{\mathrm{cl}}^2 \approx f(n_{\mathrm{co}}^2 - n_{\mathrm{ho}}^2)$ is proportional, at first order, to f and, therefore, the *material* scale is just given by the change in the filling fraction:

$$r = s_f\,. \tag{13}$$

To obtain the geometrical scale is enough to divide the radii of the equivalent step-index models of the scaled and unscaled PCFs:

$$s = s_g\left(\frac{\Lambda - \sqrt{s_f}a}{\Lambda - a}\right). \tag{14}$$

As in Fig. 1, in Fig. 2 we compare the variation of n_{eff}, n_{g} and β_2 due to several scalings, but here of a PCF characterized by $\Lambda = 2.3\,\mu$m and $a = 0.3\,\mu$m. Note that both scale factors, s_g and s_f, provide excellent estimations of the dispersive behavior of different optical properties for the design of PCFs. Even though the precision of these estimates could be further improved by means of a more accurate model for the effective step-index fiber [26,27], the results obtained in the next section indicate that Eqs. (13) and (14) already allow designing PCFs with the desired properties in four iterations or less.

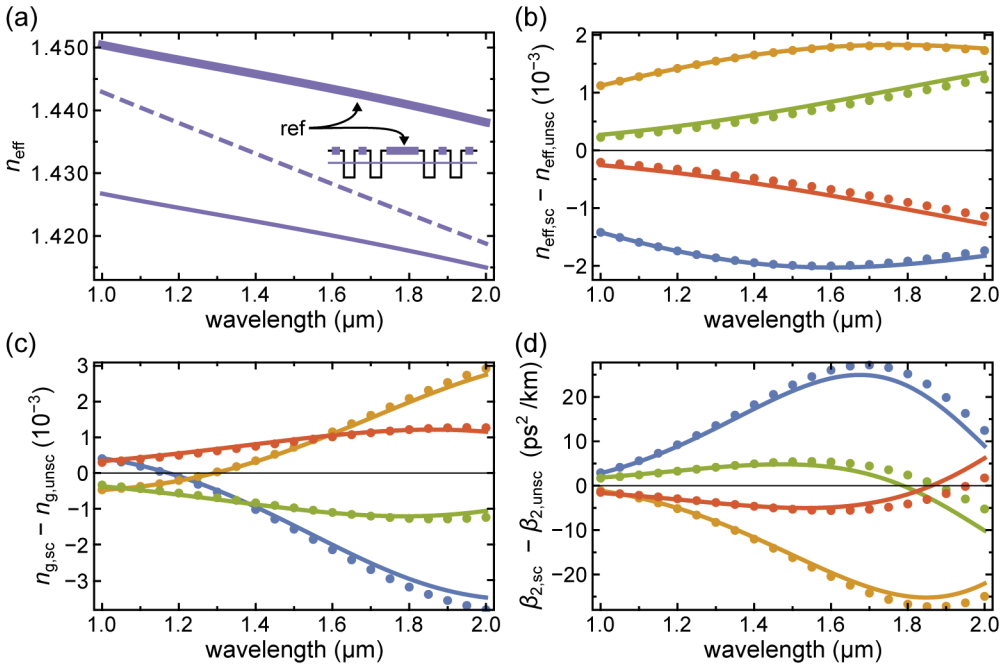

Fig. 2. (a) Effective refractive index of the fundamental mode of a PCF with $\Lambda = 2.3\,\mu$m and $a = 0.3\,\mu$m (thin dashed line), refractive index of the solid core — and matrix of the cladding — (thick solid line) and average index of the cladding (thin solid line). Variation of n_{eff} (b), n_{g} (c) and β_2 (d) when several scalings (keeping the refractive index of the solid core as the reference for internal scalings) are applied to the fiber: $(s_g, s_f) = (0.9, 1)$ [blue], $(1.1, 1)$ [orange], $(1, 0.9)$ [green], and $(1, 1.1)$ [red]; in all cases, both solving completely the mode problem (solid lines) and using the approximated analytical expressions given by Eqs. (10), (11) and (8) and the auxiliary Eqs. (13) and (14) (dotted lines). The subscripts `sc` and `unsc` refer to *scaled* and *unscaled*, respectively.

4. Design of PCFs

The optimization of the chromatic dispersion of a family of fiber designs requires the definition of a merit function evaluating the mismatch between the behavior that a particular structure presents and a target behavior. For instance, if we are interested in the optimization of the group velocity dispersion (GVD), a simple expression is the mean square difference in a certain frequency range $(\omega_1, \ldots, \omega_{N_\omega})$,

$$\chi^2(p) = \frac{1}{N_\omega} \sum_{k=1}^{N_\omega} \left[\beta_2(p;\omega_k) - \beta_2^{\text{target}}(\omega_k)\right]^2, \tag{15}$$

where p is a set of parameters defining the fiber degrees of freedom. The optimum configuration will correspond to the minimum of χ^2.

To reach that minimum, a series of approximations of χ^2 can be sequentially built and minimized [16,17]. To be more precise, in the case of optimizing PCFs with regular cladding, and given a certain configuration defined by its pitch and hole radius, (Λ, a), its GVD in the frequency range of interest must be calculated using any mode solver available (which is, in our case, the one reported in [19]). Next, Eq. (8) provides excellent estimations of the GVD for scaled configurations, $\beta_{2[sr]}$, around the unscaled one, and allows to define an approximation of

OSA CONTINUUM

the merit function,

$$\chi^2_{\mathrm{loc}}(s_f, s_g) = \frac{1}{N_\omega} \sum_{k=1}^{N_\omega} \left[\beta_{2[sr]}(\omega_k) - \beta_2^{\mathrm{target}}(\omega_k)\right]^2, \tag{16}$$

where $r = s_f$ and $s = s_g(\Lambda - \sqrt{s_f}a)/(\Lambda - a)$ [Eqs. (13) and (14)]. The values of the scale factors s_f and s_g that minimize χ^2_{loc} determine the scalings that must be applied to the initial configuration in order to get a new configuration: $(\Lambda, a) \rightarrow (\Lambda', a') = (s_g\Lambda, s_g\sqrt{s_f}a)$. This new configuration is expected to present a dispersion closer to the target and can be used as the starting point for a new iteration of the design procedure.

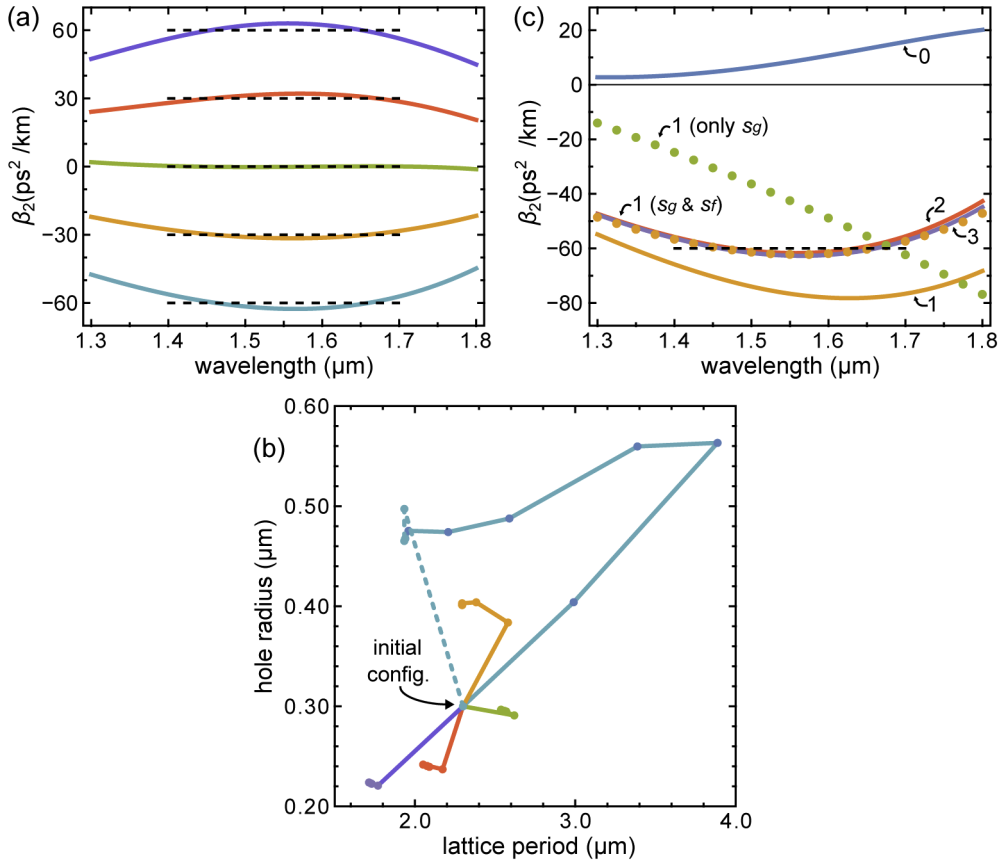

Fig. 3. (a) Dispersion of five optimized PCF designs [colored solid lines] achieved considering as target dispersions five flattened dispersion profiles with $\beta_2 = 0, \pm 30$ and $\pm 60\,\mathrm{ps^2km^{-1}}$, respectively, in the wavelength range [1.4, 1.7] μm [black dashed lines]. (b) Evolution of the geometrical parameters during the optimization procedure of the examples shown in (a) [marked with the same colors] (see details in the text). (c) Chromatic dispersion curves [colored solid lines] obtained along the free-of-constraints optimization towards the target $\beta_2 = -60\,\mathrm{ps^2km^{-1}}$ [black dashed line]. Initial estimates based on Eq. (8) restricted to $s_f = 1$ (i.e., only s_g is adjusted) [green dotted line] and unrestricted (i.e., both s_g and s_f are adjusted) [orange dotted line].

In order to illustrate our approach, we plot, in Fig. 3(a), five different examples of the design processes of PCFs with flattened dispersion profiles over 300 nm, in the range $1.4\,\mu\mathrm{m} \leq \lambda \leq 1.7\,\mu\mathrm{m}$ [$\beta_2(\omega) = 0, \pm 30$ and $\pm 60\,\mathrm{ps^2km^{-1}}$; dashed lines in Fig. 3(a)]. For all five cases, we start

OSA CONTINUUM

from the same inital configuration, hence showing this choice is not particularly relevant. In our calculations, we have used the Sellmeier coefficients for silica reported in Ref. [28]. In these examples, 7 wavelengths in the above range are considered as the points used for evaluating the approximation of the merit function [Eq. (16)]. In order to ensure that the procedure converges properly, it is sometimes convenient to moderate the speed of convergence. In Fig. 3(b) [solid lines], the evolution of the design parameters at each step along the procedure is shown, in which we have allowed variations up to 30 % in each step and we consider the process has converged when the predicted scalings (s_f, s_g) would imply changes for the next iteration smaller than 0.1 %. Even so, in those cases with $\beta_2(\omega) = 0, \pm 30$ and $+60\,\mathrm{ps^2km^{-1}}$ as target, convergence is achieved in four iterations or less.

Figure 3(b) also shows that, when $\beta_2(\omega) = -60\,\mathrm{ps^2km^{-1}}$ is targeted, the convergence process do not initially approach the optimal configuration, which is in contrast to the other optimizations. Although after eight iterations good convergence is still achieved, the evolution has not been as fast as in our other designs. However, if no restrictions are imposed on the scale factors at each iteration, convergence is achieved in less than four iterations, as shown in Figs. 3(b) [blue dashed line] and 3(c) [colored solid lines]. To highlight the importance of the material scaling transformation, we also compare in Fig. 3(c), for the first iteration, the estimated dispersion profiles obtained through only geometrical scaling [green dotted curve] and both geometrical and material scalings [orange dotted curve]. This example also points out the usefulness of our scaling transformations in any waveguide design procedure for finding appropriate approximations.

Finally, we also apply our approach to triangular PCFs with a high and negative dispersion slope, namely, one order of magnitude larger than in standard fibers. The potential applications of these chromatic dispersion profiles range from third-order-dispersion compensation [29] or spectral shaping [30] to dispersive wave emission in the normal [8,31] or anomalous dispersion regime [32], or novel bound states in mode-locked fiber lasers [33]. Accordingly, we set $\beta_2 = \pm 30\,\mathrm{ps^2km^{-1}}$ at 1.55 μm and $\beta_3 = -1\,\mathrm{ps^3km^{-1}}$ in the range $1.53\,\mu\mathrm{m} \le \lambda \le 1.57\,\mu\mathrm{m}$ as our new targets and repeated the process explained previously. The optimized designs present, for the solutions with negative and positive dispersion at 1.55 μm, a pitch and a hole radius $(\Lambda, a) = (1.212, 0.555)\,\mu\mathrm{m}$ and $(1.207, 0.467)\,\mu\mathrm{m}$, respectively. The results are plotted in Fig. 4.

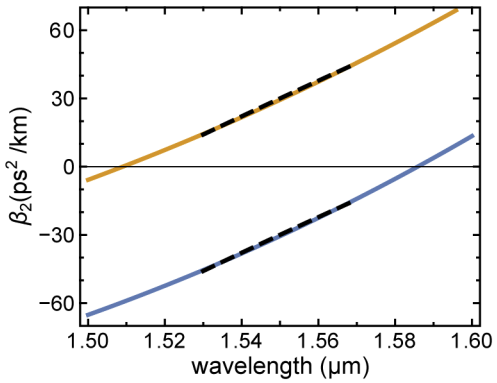

Fig. 4. Dispersion of two optimized PCF designs [colored solid lines] achieved considering as target two linear dispersion profiles in the wavelength range [1.53, 1.57] μm [black dashed lines] with $\beta_2 = \pm 30\,\mathrm{ps^2km^{-1}}$ and $\beta_3 = -1\,\mathrm{ps^3km^{-1}}$ at 1.55 μm (see details in the text).

5. Conclusions

The development of approximated analytical expressions for the mode effective index, the group index and the chromatic dispersion of scaled fibers is a powerful tool. Once a rigorous solution is

OSA CONTINUUM

known for a given fiber, the reported expressions provide an accurate evaluation of the mode parameters in the neighborhood defined by geometry and material scaling. Our results can push forward the efficiency of the designing tools of special optical fibers and even integrated waveguides, as we illustrate here with the design of a flattened dispersion PCF. In addition, our analytical expressions can benefit other applications areas such as the comparison of specific experimental results with a theoretical model that may require adjusting the geometry and materials values of a given guiding system.

Funding

Ministerio de Ciencia e Innovación and European Regional Development Fund (PDI2019-104276RB-I00); Conselleria d'Innovació, Universitats, Ciència i Societat Digital (PROMETEO/2019/048).

Acknowledgments

A. Tashtush acknowledges financial support from the Generalitat Valenciana — Santiago Grisolía doctoral fellowship (GRISOLIAP/2015/036). D. Castelló-Lurbe acknowledges financial support from the Research Foundation-Flanders (FWO) — postdoctoral fellowship (147788/12ZN720N).

Disclosures

The authors declare no conflicts of interest.

References

1. N. Ishikura, R. Hosoi, R. Hayakawa, T. Tamanuki, M. Shinkawa, and T. Baba, "Photonic crystal tunable slow light device integrated with multi-heaters," Appl. Phys. Lett. **100**(22), 221110 (2012).
2. M. A. Foster, A. C. Turner, J. E. Sharping, B. S. Schmidt, M. Lipson, and A. L. Gaeta, "Broad-band optical parametric gain on a silicon photonic chip," Nature **441**(7096), 960–963 (2006).
3. A. C. Turner-Foster, M. A. Foster, R. Salem, A. L. Gaeta, and M. Lipson, "Frequency conversion over two-thirds of an octave in silicon nanowaveguides," Opt. Express **18**(3), 1904–1908 (2010).
4. X. Liu, B. Kuyken, G. Roelkens, R. Baets, R. M. Osgood Jr., and W. M. J. Green, "Bridging the mid-infrared-to-telecom gap with silicon nanophotonic spectral translation," Nat. Photonics **6**(10), 667–671 (2012).
5. L. Yin, Q. Lin, and G. P. Agrawal, "Soliton fission and supercontinuum generation in silicon waveguides," Opt. Lett. **32**(4), 391–393 (2007).
6. R. Halir, Y. Okawachi, J. S. Levy, M. A. Foster, M. Lipson, and A. L. Gaeta, "Ultrabroadband supercontinuum generation in a CMOS-compatible platform," Opt. Lett. **37**(10), 1685–1687 (2012).
7. J. J. Miret, E. Silvestre, and P. Andrés, "Octave-spanning ultraflat supercontinuum with soft-glass photonic crystal fibers," Opt. Express **17**(11), 9197–9203 (2009).
8. D. Castelló-Lurbe and E. Silvestre, "Supercontinuum generation in silicon waveguides relying on wave-breaking," Opt. Express **23**(20), 25462–25473 (2015).
9. A. Ferrando, E. Silvestre, P. Andrés, J. J. Miret, and M. V. Andrés, "Designing the properties of dispersion-flattened photonic crystal fibers," Opt. Express **9**(13), 687–697 (2001).
10. M. D. Nielsen and N. A. Mortensen, "Photonic crystal fiber design based on the *V*-parameter," Opt. Express **11**(21), 2762–2768 (2003).
11. K. Saitoh and M. Koshiba, "Empirical relations for simple design of photonic crystal fibers," Opt. Express **13**(1), 267–274 (2005).
12. F. Poletti, V. Finazzi, T. M. Monro, N. G. T. Broderick, V. Tse, and D. J. Richardson, "Inverse design and fabrication tolerances of ultra-flattened dispersion holey fibers," Opt. Express **13**(10), 3728–3736 (2005).
13. S. Jensen and O. Sigmund, "Topology optimization for nanophotonics," Laser Photonics Rev. **5**(2), 308–321 (2011).
14. S. Molesky, Z. Lin, A. Y. Piggott, W. L. Jin, J. Vucković, and A. W. Rodriguez, "Inverse design in nanophotonics," Nat. Photonics **12**(11), 659–670 (2018).
15. W. Q. Zhang, S. Afshar V., and T. M. Monro, "A genetic algorithm based approach to fiber design for high coherence and large bandwidth supercontinuum generation," Opt. Express **17**(21), 19311–19327 (2009).
16. E. Silvestre, T. Pinheiro-Ortega, P. Andrés, J. J. Miret, and Á. Coves, "Differential toolbox to shape dispersion behavior in photonic crystal fibers," Opt. Lett. **31**(9), 1190–1192 (2006).
17. D. Castelló-Lurbe, V. Torres-Company, and E. Silvestre, "Inverse dispersion engineering in silicon waveguides," J. Opt. Soc. Am. B **31**(8), 1829–1835 (2014).

OSA CONTINUUM

18. J. Lægsgaard, A. Bjarklev, and S. E. Barkou Libori, "Chromatic dispersion in photonic crystal fibers: fast and accurate scheme for calculation," J. Opt. Soc. Am. B **20**(3), 443–448 (2003).
19. E. Silvestre, T. Pinheiro-Ortega, Pedro Andrés, J. J. Miret, and A. Ortigosa-Blanch, "Analytical evaluation of chromatic dispersion in photonic crystal fibers," Opt. Lett. **30**(5), 453–455 (2005).
20. J. D. Joannopoulos, S. G. Johnson, R. D. Meade, and J. N. Winn, *Photonic Crystals: Molding the Flow of Light* (Princeton, 2008).
21. T. A. Birks, D. M. Bird, T. D. Hedley, J. M. Pottage, and P. St. J. Russell, "Scaling laws and vector effects in bandgap-guiding fibres," Opt. Express **12**(1), 69–74 (2004).
22. A. W. Snyder and D. J. Love, *Optical Waveguide Theory* (Chapman and Hall, 1983).
23. B. Feigel, D. Castelló-Lurbe, H. Thienpont, and N. Vermeulen, "Opportunities for visible supercontinuum light generation in integrated diamond waveguides," Opt. Lett. **42**(19), 3804–3807 (2017).
24. D. E. Aspnes, "Local-field effects and effective-medium theory: A microscopic perspective," Am. J. Phys. **50**(8), 704–709 (1982).
25. E. Silvestre, P. St. J. Russell, T. A. Birks, and J. C. Knight, "Analysis and design of an endlessly single-mode finned dielectric waveguide," J. Opt. Soc. Am. A **15**(12), 3067–3075 (1998).
26. K. N. Park and K. S. Lee, "Improved effective-index method for analysis of photonic crystal fibers," Opt. Lett. **30**(9), 958–960 (2005).
27. Y. F. Li, Y. H. Yao, M. L. Hu, L. Chai, and C. Y. Wang, "Improved fully vectorial effective index method for photonic crystal fibers: evaluation and enhancement," Appl. Opt. **47**(3), 399–406 (2008).
28. J. W. Fleming, "Material and mode dispersion in GeO_2 ·B_2O_3 ·SiO_2 glasses," J. Am. Ceram. Soc. **59**(11-12), 503–507 (1976).
29. C. Fortier, J. Fatome, S. Pitois, J.-P. Couvercelle, M.-L. Leonard, E. Pincemin, and F. Reynaud, "Stretched fibre based dispersion compensating module for ultra high-speed telecommunication systems," Electron. Lett. **44**(17), 1025–1027 (2008).
30. D. Castelló-Lurbe, P. Andrés, and E. Silvestre, "Dispersion-to-spectrum mapping in nonlinear fibers based on optical wave-breaking," Opt. Express **21**(23), 28550–28558 (2013).
31. K. E. Webb, Y. Q. Xu, M. Erkintalo, and S. G. Murdoch, "Generalized dispersive wave emission in nonlinear fiber optics," Opt. Lett. **38**(2), 151–153 (2013).
32. D. Castelló-Lurbe, N. Vermeulen, and E. Silvestre, "Towards an analytical framework for tailoring supercontinuum generation," Opt. Express **24**(23), 26629–26645 (2016).
33. Y. Wang, J. Li, L. Hong, G. Li, F. Liu, X. Zhou, and Y. Liu, "Coexistence of dissipative soliton and stretched pulse in dual-wavelength mode-locked Tm-doped fiber laser with strong third-order dispersion," Opt. Express **26**(14), 18190–18201 (2018).